Brief Papers

A Low Noise, High Resolution Silicon Temperature Sensor

Kenneth S. Szajda, Charles G. Sodini, and H. Frederick Bowman

Abstract— **High resolution temperature measurement is essential for determination of blood perfusion in biomaterials. A compact, low noise, high resolution temperature sensor designed for use in an invasive tissue property measurement probe is presented. The circuit is based on traditional proportional-to-absolute-temperature (PTAT) principles. A feedback technique is used to improve linearity and reduce noise. Data from test chips shows temperature resolution of 3 m°C. The chips were fabricated using a 1.75 μm double poly, single metal modified CMOS process designed for this project.**

I. Introduction

THE quantification of volumetric blood flow (perfusion) is essential for the optimization of nonsurgical treatment of tumors. The effectiveness of chemotherapy, radiotherapy, immunotherapy, and hyperthermia is strongly influenced by local tissue perfusion since this is the primary pathway for heat removal and oxygen and nutrient supply. Invasive perfusion measurement is typically performed by applying a small local temperature step (3–6°C) to the tissue using a resistive heater or thermistor and monitoring the power required to maintain the temperature increment. Previous analytical work [1] has demonstrated that precise knowledge of the temperature increment is essential for accurate determination of perfusion from the measured power data. Fig. 1 shows the relationship between the percentage uncertainty in perfusion as a function of perfusion for various temperature resolutions. Tissue flow rates can be as low as 5 ml/100 g-min; perfusion measurement to ±5% at this level requires a temperature resolution on the order of 0.1%, or, for a nominal 5°C increment, 5 m°C.

The best perfusion measurement systems currently available use thermistors for both heating and temperature monitoring, but are limited by large probe size (approximately 1 mm diameter) and the signal corruption that occurs between the measurement site and remotely located signal detection circuitry. Semiconductor-based sensors could potentially alleviate both of these problems. Previous work on silicon temperature sensors has focused on medium resolution, high dynamic range

Manuscript received March 17, 1995; revised January 29, 1996. This work was supported by the National Cancer Institute of the National Institutes of Health under contract # CA31303.

K. S. Szajda was with the Department of Electrical Engineering and Computer Science, Massachusetts Institute of Technology, Cambridge, MA 02139 USA. He is currently with the Harvard-MIT Division of Health Sciences and Technology and LSI Logic Corp., Waltham, MA 02154 USA.

C. G. Sodini is with the Department of Electrical Engineering and Computer Science, Massachusetts Institute of Technology, Cambridge, MA 02139 USA.

H. F. Bowman is with the Harvard-MIT Division of Health Sciences and Technology, Cambridge, MA 02139 USA.

Publisher Item Identifier S 0018-9200(96)06473-6.

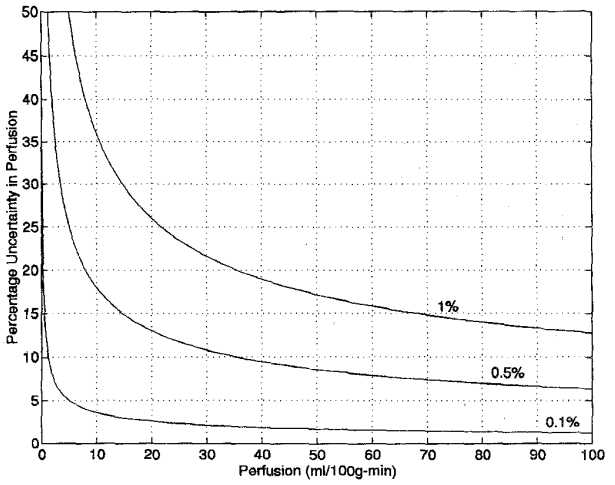

Fig. 1. Uncertainty in perfusion as a function of perfusion for various temperature resolutions.

specifications [2] and [3]. Most of the few sensors built for biomedical applications are limited by the signal excitation or detection circuits [4]–[6]. As the first step toward realizing a silicon perfusion sensor, a high resolution temperature sensor has been designed and fabricated. In addition to its small size (0.14 mm^3 total volume), the sensor also achieves 3 m°C temperature resolution over the biomedical temperature range of interest (30–50°C).

II. Theory

The temperature behavior of the forward voltage of a p-n junction diode can be derived from the diode current equation

$$I_D = I_S\,(e^{V_D/V_{TH}} - 1) \tag{1}$$

where I_D is the diode current, I_S is the reverse saturation current, V_D is the diode voltage, and V_{TH} is the thermal voltage (kT/q). The temperature behavior of the saturation current I_S is [7]

$$I_S = AT^{\beta}e^{-V_{go}/V_{TH}} \tag{2}$$

where A and β are (temperature independent) material dependent parameters, and V_{go} is the bandgap voltage of silicon at absolute zero, approximately 1.205 V. Assume that the temperature dependence of the excitation current is of the form

$$I_D = BT^{\alpha} \tag{3}$$

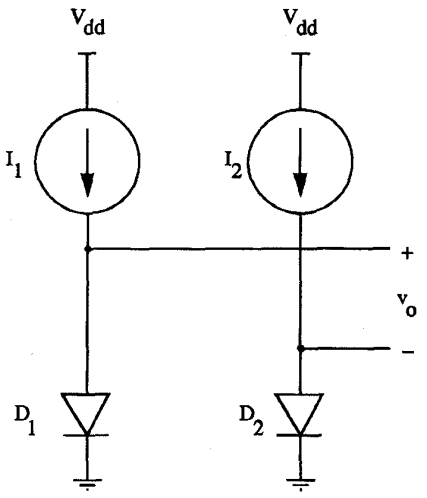

Fig. 2. Difference-of-v_D PTAT circuit.

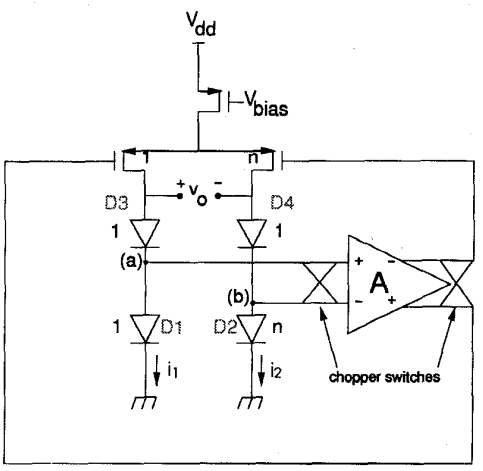

Fig. 3. Temperature sensor simplified schematic.

where B is again a temperature independent process parameter.

The output of the traditional proportional-to-absolute-temperature (PTAT) circuit shown in Fig. 2 is given by

$$V_o = V_{D1} - V_{D2}$$
$$V_o = V_{TH} \ln\left(\frac{A_2 B_1}{A_1 B_2}\right) \tag{4}$$

where it is assumed that the temperature behavior of the driving sources are the same, as is the temperature behavior of the reverse saturation current. This relationship between the output voltage and temperature is linear; rearranging the equation gives explicitly

$$T = \frac{V_o}{\ln\left(\frac{A_2 B_1}{A_1 B_2}\right)} \cdot \left(\frac{q}{k}\right) \tag{5}$$

$$T = \left(\frac{q}{k}\right) \cdot \frac{V_o}{\ln\left(\frac{I_1}{I_2}\right)}. \tag{6}$$

A simplified schematic of the improved sensor design is shown in Fig. 3. At its core is the fundamental PTAT circuit, namely, two diodes that are excited unequally.

Assume for the moment that the op-amp is ideal. In this case, the voltage at node (a) is equal to that at node (b). From the diode equation, it is clear that

$$\frac{kT}{q} \log\left(\frac{I_1}{I_{s1}}\right) = \frac{kT}{q} \log\left(\frac{I_2}{I_{s2}}\right). \tag{7}$$

Since the diode areas are in a $1 : n$ ratio, $I_{s2} = nI_{s1}$, and

$$\frac{I_2}{I_1} = n. \tag{8}$$

The excitation current ratio is therefore determined solely by the geometry ratio of the diodes. Any mismatch in the diode area ratio due to normal process variation appears as a fixed ratio "offset" that can very easily be calibrated. With a fixed, temperature independent current ratio, the voltage across the two sense diodes is proportional to absolute temperature and is given by

$$v_d = \frac{kT}{q} \log(n). \tag{9}$$

III. Sensing Circuit Nonidealities

A. Temperature Coefficient Errors

In the initial derivation of the linear output of the PTAT, several temperature independent parameters were introduced: A, B, α, and β. Although different values for A and B are clearly necessary in each leg of the PTAT (since the excitation currents and/or the diode areas must be different to generate an output voltage), it was assumed that the values of α and β were equal in both legs of the circuit. There is no guarantee that these parameters will indeed be equal. As a result, a nonlinearity will result in the output characteristic.

In terms of average and difference parameters, it is found that

$$V_o = V_{D1} - V_{D2}$$
$$= V_{TH} \ln\left(\frac{B_1}{A_1} \cdot \frac{A_2}{B_2}\right) + V_{TH}(\Delta\alpha - \Delta\beta) \ln(T). \tag{10}$$

This result shows that it is not strictly necessary that $\Delta\alpha = 0$ and $\Delta\beta = 0$ for the output to be linear. The correct, slightly looser constraint is that $\Delta\alpha = \Delta\beta$. Since, by definition, all of the geometry and temperature coefficient parameters (α, β, A, B) are temperature independent, the nature of any nonlinearity that does occur is very well described, namely, it is of the form $T \ln(T)$.

B. Device Mismatch/Op-Amp Gain Errors

Another potential source of error comes from the fact that the operational amplifier does not have infinite gain, and, therefore, the two input terminals v_+ and v_- are not necessarily equal, as was assumed in the derivation of the sensor output characteristic.

The most straightforward way to minimize this error is to guarantee that the differential op-amp output voltage is

nominally zero. If this is the case, then the op-amp inputs will be equal independent of the op-amp gain. Since the desired current ratio is $1 : n$, this condition can be brought about by appropriately modifying the geometry ratios of the differential pair transistors. Since we know that the ratio $I_2/I_1 = n$, it follows immediately that for zero differential op-amp output it is necessary that

$$\frac{\left(\frac{W}{L}\right)_2}{\left(\frac{W}{L}\right)_1} = n \tag{11}$$

as indicated in Fig. 3.

This eliminates (to first order) errors associated with the finite gain; however, normal process variation will guarantee that the geometry ratios are never exactly $1 : n$, which will require a nonzero differential op-amp output voltage. Therefore proper consideration of the op-amp gain error requires accounting for the nonidealities of the differential pair transistors also.

The best way to examine these effects is to consider the errors as small perturbations from the ideal situation. Assuming that the current error induced by the nonzero differential voltage difference at the op-amp input is small, it can be shown that the differential voltage error at the differential pair inputs is approximately

$$\Delta V \approx -\Delta V_T + \frac{c}{n}\sqrt{\frac{I_o}{2nk'\left(\frac{W}{L}\right)_1}} \tag{12}$$

where n is the desired (ideal) current ratio, c is the ratio mismatch between $(W/L)_1$ and $(W/L)_2$, and ΔV_T is the threshold mismatch in the differential pair.

There are several important points to note. First, the error voltage is linear with both ΔV_T and c. Second, the error contribution due to the threshold mismatch is on the same order as the threshold mismatch itself. Third, the error due to (W/L) ratio mismatch is roughly the gate drive times the percentage ratio error (in fact, it is a factor of $\sqrt{n}$ less than that). Thus, for typical process mismatch parameters, the error voltage will indeed be small. For a current ratio of ten, for example, with $(W/L)_1 = 25/3$, $I_o = 44\,\mu$A (corresponding to $I_1 = 4\,\mu$A and $I_2 = 40\,\mu$A), an op-amp gain of 10^5, $\Delta V_T = -10$ mV[1] and $c = 0.1$, one finds that $\Delta V = 109$ nV when referred to the op-amp inputs. Finally, it is the drift in this voltage with temperature that results in a measurement error; for a 10% drift over the biomedical temperature range the error contribution is approximately 10.9 nV.

C. Circuit/Device Noise

The third major error contribution is due to device noise. The device noise could become a dominant error source because of the high resolution requirements of the sensor. Fig. 4 shows the sensing circuit with all noise sources present.

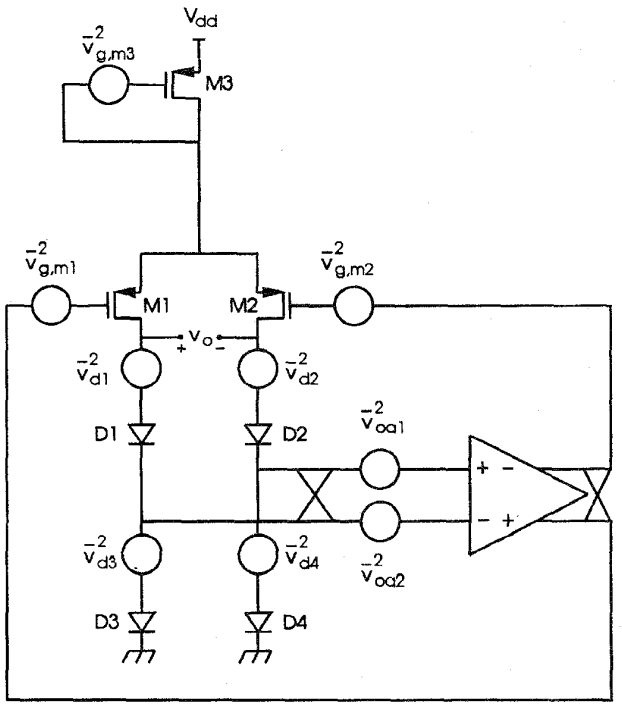

Fig. 4. Sensing circuit with noise sources.

The total noise of each MOSFET consists of flicker and thermal noise components [8].

The total noise of the MOS transistor over a bandwidth from f_l to f_h is

$$v_{n,\,\mathrm{tot}} = \sqrt{\frac{\gamma 4kTg_{d0}}{g_m^2}(f_h - f_l) + \frac{K}{WL(1-\alpha)}[f_h^{1-\alpha} - f_l^{1-\alpha}]} \tag{13}$$

where k is Boltzmann's constant, T is the absolute temperature (in Kelvin), α is the flicker noise exponent ($\approx$1), g_m is the transconductance of the device, g_{d0} is the device channel conductance at $V_{ds} = 0$, and K is the flicker noise coefficient, a process dependent parameter.[2] The thermal noise coefficient γ is bias dependent, and varies from $\gamma = 1$ at $V_{ds} = 0$ to $\gamma = 2/3$ in saturation. It has been assumed that $\alpha \neq 1$.

The total noise of each of the three MOS transistors can be computed using the above formula. For each of the differential pair devices, the noise is divided by the open loop gain of the amp when it is referred to the output of the sensing circuit. This reduction occurs because of the feedback action. The noise from the current source transistor is, in theory, not reflected in the output noise, as it appears as a common mode noise.

The input referred noise of the operational amplifier $\overline{v_{oa}^2}$ is a potentially significant source of error, since noise at the operational amplifier inputs is directly reflected in the sensor output voltage. Because of the large low-frequency flicker noise associated with MOS devices, chopper modulation is

[1] Because the differential pair is purposely mismatched, the sign of ΔV_T is important. The error is largest when ΔV_T is negative.

[2] The dependence of the flicker noise on C_{ox} is lumped into K for this analysis.

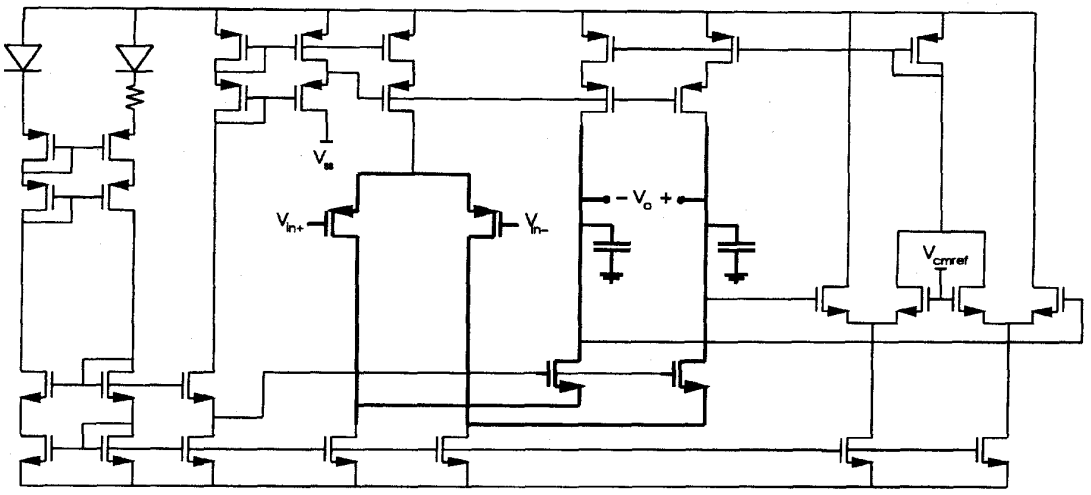

Fig. 5. Fully differential folded cascode op-amp.

used to move this noise out of the frequency range of interest as indicated in Fig. 3.

The noise contributed by the op-amp is therefore limited to its input referred thermal noise. Since this is strongly dependent on the op-amp topology, an exact formulation of this error source is not given here. The important conclusions, however, are that the $1/f$ noise component is eliminated by chopper modulation, and that the thermal noise is unattenuated by the loop and appears directly at the sensor output. This is the noise component that must be minimized in the design of the operational amplifier. For the implementation used, the total circuit/device noise contribution is approximately 12.3 nV.

D. Diode Noise

The last major noise source is due to the diodes themselves, both the ones used for sensing and the ones used for current ratio control. Noise from these devices is unattenuated by the loop. As a result, these diodes become the dominant noise generator of the entire sensor.

The general form of the total low frequency diode noise over a frequency range f_l to f_h is therefore

$$v_d^2 = \frac{K_d I_d}{A(1-\gamma)} \left[\frac{1}{f_h^{\gamma-1}} - \frac{1}{f_l^{\gamma-1}} \right] \tag{14}$$

for an individual diode, where K_d is the process-dependent flicker noise coefficient, I_d is the diode current, A is the diode area, and γ is the flicker noise exponent. At low frequencies, the thermal noise contribution is negligible.

Since four diodes are used in the sensing circuit, the total noise contribution due to the four diodes is the sum (in the mean-square sense) of the individual contributions, and

$$v_{\text{diodes, tot}} = \sqrt{v_{d1}^2 + v_{d2}^2 + v_{d3}^2 + v_{d4}^2}. \tag{15}$$

For this implementation, the total diode noise contribution is approximately 65.8 nV. Noise from all sources translates into a minimum theoretical resolution of 0.34 m°C.

IV. Experimental Results

A. Test Setup

The circuit of Fig. 3 has been fabricated using a 2-poly, single metal modified CMOS process developed for this purpose. The sensing and current control diodes are formed by diode connecting NPN devices. The NPN transistors are triple-diffused, vertical devices that show excellent diode behavior ($n \approx 1$) over nearly eight decades of current. The op-amp is a fully differential folded cascode (Fig. 5); it has a dc gain of 100 dB and a unity gain bandwidth of 2.2 MHz (19.2 pF load). The chopping frequency is 24 kHz. The circuit uses a current ratio of 10 : 1, for a linear output voltage signal that changes by 198 μV/°C.

A stable environment for temperature measurement was created using a circulating water bath. The temperature of the bath was controlled using a Techne TU-19 heater/controller. The chips themselves were mounted in 40 pin DIP's for testing. Two thermistors, calibrated to ±3 m°C, were attached to the ceramic chip carrier so that the actual carrier temperature could be monitored. Since the thermal conductivity of the silicon/ceramic system is much larger than any other material used in the system, the carrier temperature is an excellent measure of the chip temperature. The two thermistors were separated by a known fixed distance, which made possible quantification and correction for any thermal gradients that might be present due to temperature stratification in the bath.

The chip/thermistor assembly was placed in a small waterproof plastic bag that was sealed and immersed in the water bath. The plastic "capsule" was clamped under the surface of the water to prevent motion during the measurements and flotation caused by residual air in the bag. Analog data from the sensor was digitized on-chip using a custom fourth-order oversampled modulator [9]. Digital data generated by the chip under test was passed to a personal computer. Temperature recordings from the thermistors were taken using a thermistor-based temperature measurement system of resolution 3 m°C (TDP-100, Thermal Technologies Inc., Cambridge, MA) cal-

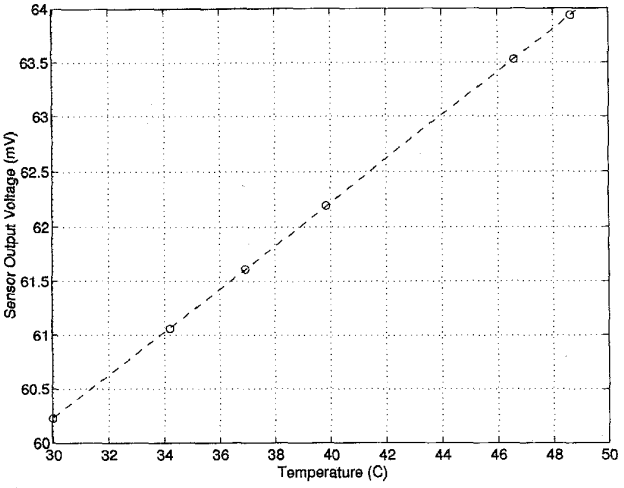

Fig. 6. Measured temperature sensor output characteristic.

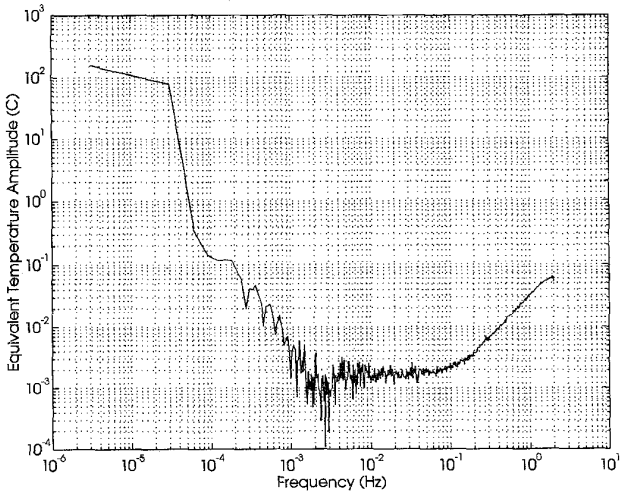

Fig. 7. 90 min temperature step experiment output spectrum.

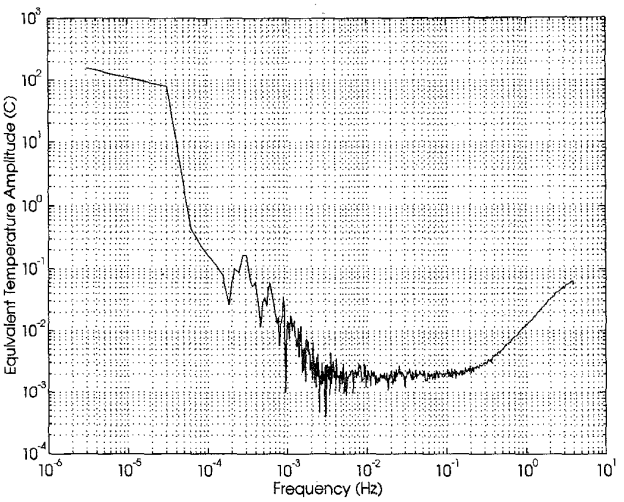

Fig. 8. 60 min temperature step experiment output spectrum.

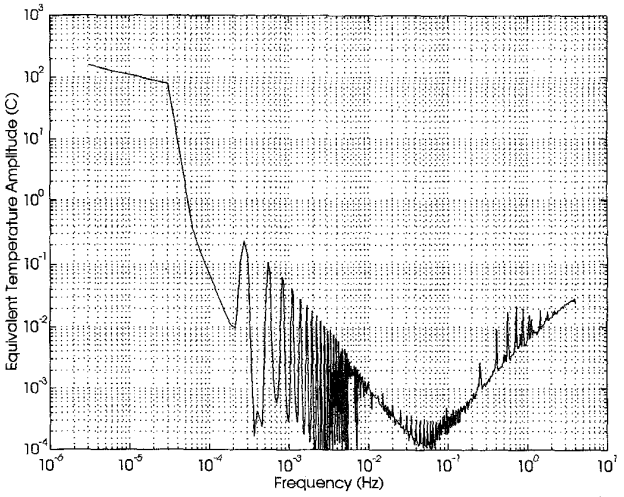

Fig. 9. Spectrum of "noiseless" 60 min step experiment.

ibrated against a precision thermometer traceable to an NIST standard. This system was connected to a second personal computer, where the measurements were displayed.

B. Measurement Results

The first test performed measured the dc temperature characteristics of the sensor over the biological temperature range of interest. To do this, the water bath temperature was fixed and bits were recorded over a long time period, approximately 30 min. The chip carrier temperature during this time was monitored by the thermistor probes. At the end of the 30 min period, the average value of the bits was computed and the steady temperature of the two thermistors was noted. The approximate chip temperature T_c was computed by extrapolation from the two thermistor measurements. The equivalent temperature sensor output voltage v_o was calculated from the pulse density and knowledge of the system construction. This v_o, T_c pair was one data point. The water bath temperature was changed, and the chip temperature allowed to reach thermal equilibrium; this process took approximately 1 h (due to the large volume of water in the bath) and was verified by the thermistors. This measurement process was repeated several times at different temperatures to produce a total of six data points.

The results of this experiment are shown in Fig. 6. As expected, the nominal sensor output voltage is approximately 60 mV $[\approx(kT/q)\ \ln 10]$. Although calculations from the best-fit line show linearity of approximately 35 m°C, this value is subject to error due to the ±3 m°C uncertainty in both thermistor measurements and, correspondingly, in calculation of the actual chip temperature from the thermal gradient. Another source of error is the water bath temperature controller, which controls the temperature to ±20 m°C at its interrogation point. For this reason, no conclusive figure on the inherent linearity of the circuits can be determined from this experiment.

The second test was the most critical and was used to evaluate the fundamental thermal resolution of the system as designed. A thermal "staircase" function was applied to the

system and the spectrum of the output bits examined. After allowing initial equilibration of the test setup, the temperature of the water bath was stepped periodically over the course of a day. For this experiment, one of the most important parameters was the time interval at which the steps were applied, since the spectral purity of the staircase function depends on the periodicity in the applied steps. Two separate tests were performed using periods of 60 and 90 min between steps to insure that the period of the steps did not affect the system noise performance.

The results of these tests are shown in Figs. 7 (90 min steps) and 8 (60 min steps). For reference, Fig. 9 shows the spectrum of a simulated noiseless staircase with 60 min steps; the transform for the 90 min steps would have the same shape with a different periodicity of the humps. The Fourier transform of the measured output bits should show the spectrum of the input staircase function superimposed on the system noise spectrum. A comparison of Fig. 8 with Fig. 9 clearly shows the "humps" that occur at the fundamental step frequency (0.28 mHz for 60 min steps, 0.19 mHz for 90 min steps) and harmonics. At moderate frequencies, the magnitude of the harmonics is very small and the transform is dominated by the noise floor of the system. The rise in the spectrum at higher frequencies is due to aliasing from the data acquisition system. From this test, the resolution of the test chips is approximately 3 m°C.

V. Conclusion

A low noise, high resolution temperature sensor has been presented. The circuit, which is based on the traditional PTAT topology, uses feedback to minimize noise and maintain linear behavior over the biomedical temperature range of interest. Prototype chips have shown a temperature resolution of 3 m°C.

Acknowledgment

The assistance of the staff of the Microsystems Technology Labs at MIT in the fabrication of the chips is greatly appreciated.

References

[1] H. F. Bowman, T. A. Balasubramaniam, and M. Woods, III, "Determination of tissue perfusion from *in vivo* thermal conductivity measurements," in *Proc. ASME Winter Ann. Mtg.*, American Society of Mechanical Engineers, Dec. 1977, paper 77-WA/HT-40.

[2] G. C. M. Meijer, "Thermal sensors based on transistors," *Sensors and Actuators,* vol. 10, pp. 103–125, 1986.

[3] R. N. Sengupta, "A widely linear temperature to frequency converter using a thermistor in a pulse generator," *IEEE Trans. Electron Devices,* vol. 37, no. 1, pp. 62–65, Mar. 1988.

[4] P. W. Barth and J. B. Angell, "Thin linear thermometer arrays for use in localized cancer hyperthermia," *IEEE Trans. Electron Devices,* vol. ED-29, no. 1, pp. 144–150, Jan. 1982.

[5] G. C. M. Meijer, R. Van Gelder, V. Nooder, J. Van Drecht, and H. Kerkvleit, "A three-terminal integrated temperature transducer with microcomputer interface," *Sensors and Actuators,* pp. 195–206, 1989.

[6] R. C. S. Freire, S. Daher, and G. S. Deep, "A highly linear single p-n junction temperature sensor," *IEEE Trans. Instrum. Meas.,* vol. 43, no. 2, pp. 127–132, Apr. 1994.

[7] P. R. Gray and R. G. Meyer, Eds., *Analysis and Design of Analog Integrated Circuits.* New York: Wiley, 1984.

[8] A. van der Ziel, *Noise in Solid State Devices and Circuits.* New York: Wiley, 1986.

[9] K. S. Szajda, "A high resolution integrated circuit biomedical temperature sensing system," Ph.D. thesis, Massachusetts Institute of Technology, Feb. 1995.